Engineering Transactions, **70**(2): 157–181, 2022, doi: 10.24423/EngTrans.1645.20220613
Institute of Fundamental Technological Research Polish Academy of Sciences (IPPT PAN)
Université de Lorraine • Poznan University of Technology

Research Paper

Comparative Assessment of Commonly Used Concrete Damage Plasticity Material Parameters

Hasan AL-RIFAIE*, Darbaz MOHAMMED

Institute of Structural Analysis, Poznan University of Technology
Poznan, Poland

*Corresponding Author e-mail: hasan.al-rifaie@put.poznan.pl

The non-homogeneous and non-linear mechanical behaviour of concrete complicates the numerical simulations of its corresponding material model. The concrete damaged plasticity (CDP) model is one of the most popular constitutive models for concrete. State-of-the-art CDP material parameters are introduced in Abaqus documentation [1], Jankowiak and Łodygowski [2], and Hafezolghorani *et al.* [3]. Accordingly, this paper presents a novel comparative study of these commonly-used concrete CDP parameters by assessing the response of plain concrete specimens under quasi-static loading conditions. The research conducts standard laboratory tests: compressive strength test of a concrete cube and three-point flexural test of a plain concrete beam. Sophisticated non-linear computational models are built using Abaqus/CAE and analysed using Abaqus/Explicit solver. The results discuss and compare deformations, damage patterns, reaction forces, compressive strength, tensile stress and modulus of rapture. The thorough study concludes that choosing CDP parameters is case-dependant and should be selected carefully.

Key words: concrete damage plasticity; compressive strength; three-point flexural test; numerical simulation; Abaqus.

1. Introduction

Concrete is a widely used and durable construction material. Nevertheless, poor resistance of plain concrete in tensile loading may limit its usage. The systematic use of steel reinforcement bars embedded in concrete produces a composite material with better resistance to tensile forces [4]. Since the 1970s, finite element analysis of concrete has significantly developed [5]. Many researchers published several reports and technical guidelines on the subject of analysing the behaviour of concrete [6–9]. However, the concrete behaviour is complex when different parameters must be taken into account during numerical analysis [10, 11]. Concrete is non-homogeneous because it is composed of different types of materials. Besides, the non-linear stress-strain relation of concrete

makes the behaviour prediction of concrete more complicated under stress conditions and strain hardening/softening [12]. Therefore, it can be difficult to accurately determine in a numerical manner the concrete damage/crack patterns. For this purpose, different constitutive models are used [13], such as concrete damage plasticity, concrete smeared cracking, Winfrith, PRM and brittle cracking [3, 14].

Szczecina and Winnicki [15] performed numerical simulations concerning uniaxial and biaxial compression and uniaxial tension of a concrete specimen sample using the CDP model implemented in Abaqus. In their model, different parameters were investigated such as the viscosity parameter, the dilation angle in the *p*-*q* plane, the flow potential eccentricity, and the ratio of initial biaxial compressive yield stress to initial uniaxial compressive yield stress. The research concluded that choosing CDP model parameters should be done very carefully.

Furthermore, the study of Jankowiak and Łodygowski [2] linked the real behaviour of concrete with its numerical modelling, and presented the requirements to identify constitutive parameters for the CDP model of concrete. The proposed CDP parameters might be used to model the behaviour of plain concrete, reinforced concrete, and other pre-stressed concrete structures in advanced stages of loadings. The paper by Fedoroff *et al.* [16] aimed to "open the black box" of the CDP model. The authors looked at the sensitivity of CDP parameters by investigating the "uniaxial tension state", the "pure shear state" and the "uniaxial confined compressive state". The research concluded that element removal criteria are crucial in simulations with fragmentation to see macroscopic crack formation [16].

Chaudhari and Chakrabarti [17] tested a numerical model of a concrete cube using the CDP model and compared it with the smeared cracking model. The concrete cube had a dimension of 150 mm, with a C3D8 element mesh type. A steel plate of thickness 25 mm was placed at the top and bottom of the cube to ensure the uniform distribution of the compressive load applied. The plate was also modelled with the same element type. The concrete material properties used were taken from Hafezolghorani *et al.* [3]. The average compressive stress $\sigma_{cu} = 30$ MPa, the ultimate strain $\varepsilon_{cu} = 0.0035$, and the strain at peak stress $\varepsilon'_0 = 0.002$. The test results of Chaudhari and Chakrabarti [17] show a perfectly nonlinear behaviour in both cases. By using the concrete damaged plasticity model of mesh size of 25 mm, the stress was found to be 32.33 MPa at 0.00195 strain, after which it started decreasing. For the smeared crack modelling, for the same mesh size, the obtained stress-strain curve gave a maximum stress of 29.39 MPa at 0.00190 strain, and then the curve showed a decreasing tendency. It can be concluded that by using the CDP model for the same mesh size, the stress-strain curve gave higher maximum stress for the CDP model than for the smeared crack model. In addition, CDP was found to be more mesh sen-

sitive than smeared crack modelling, in which less variation of stress values was observed [17].

On the other hand, WAHALATHANTRI *et al.* [18] presented a material model to simulate load-induced cracking in reinforced concrete elements in Abaqus. Two numerical material models were used and combined to simulate the stress-strain behaviour of concrete under compression, tension, and damage. The model was validated using different experimental results for the reinforced concrete (RC) beam. The finite element model of the RC beam of [18] consists of two materials: concrete and reinforcement. A value of 51.2 MPa is considered the compressive strength. Results of WAHALATHANTRI *et al.* [18] show that the crack patterns obtained from FEM followed the experiment results. The paper concluded that the material model could be applied for both reinforced and fibre-reinforced concrete crushing.

HAFEZOLGHORANI *et al.* [3] developed a simplified concrete damage plasticity (SCDP) model by combining a stress-based plasticity part with a strain-based damage model for unconfined pre-stressed concrete beam, based on a tabular format. CDP parameters were presented in the form of tables for concrete classes B20, B30, B40, and B50. A simply supported pre-stressed beam was numerically simulated with the four different concrete classes. The authors concluded that their SCDP model was a suitable solution to model the cracking and the crushing of concrete by successfully predicting the concrete damage caused by both tension and compressive stresses. Moreover, the model realistically described the transition from tensile to compressive failure, which was achieved by introducing two separate isotropic damage variables for tension and compression.

The CDP model was used for other applications, such as concrete bridge deck panels [19], FRP confined columns and beams [20, 21], fibre-reinforced concrete under impact loads [22, 23], cyclic behaviour of plain concrete [24], concrete shear capacity [25] and many more applications.

From the above-reviewed literature, it can be concluded that the CDP model is widely used to numerically predict the concrete behaviour, using few validated material parameters. However, to the authors' knowledge, a comparative assessment of the above CDP material parameters have not yet been presented in the literature. Therefore, the aim of this research is to conduct a comparative study of four commonly used CDP material parameters (Abaqus documentation [1], JANKOWIAK and ŁODYGOWSKI [2], and two models of HAFEZOLGHORANI *et al.* [3]) by assessing the compression and bending response of plain concrete specimens under quasi-static loading. The objectives are to examine the behaviour of two numerical FE models: the compressive strength test for a concrete cube and the three-point flexural test for a concrete beam. The comparison will be based on the behaviour of plain concrete specimens in compression or bending, with observing deformation values, reaction forces, crack patterns, and damage.

2. CDP material model

CDP is one of the material models in Abaqus for modelling the non-linear behaviour of concrete. CDP is based on the plasticity theory developed by Lubliner *et al.* [26]. Later, some modification was introduced by [27]. CDP can be used for static and dynamic models [28]. However, the use of CDP in high strain rate dynamic models might be problematic as it is not a rate-dependent material model. For impact simulations, modifications to the CDP model need to be done in order to account for confinement stress dependency and strain-rate dependency [29]. When loaded, the concrete shows a non-linear manner, followed by failure mechanisms of cracking in tension and crushing in compression [17]. The biaxial yield surface is a modified Drucker–Prager type function [27, 28]. The stress-strain relations are governed by scalar damaged elasticity:

$$\boldsymbol{\sigma} = (1-d)\mathbf{D}_0^{el} : \left(\boldsymbol{\varepsilon} - \boldsymbol{\varepsilon}^{pl}\right) = \mathbf{D}^{el} : \left(\boldsymbol{\varepsilon} - \boldsymbol{\varepsilon}^{pl}\right), \tag{2.1}$$

where $\boldsymbol{\sigma}$ is the Cauchy stress tensor, d is the scalar stiffness degradation variable, $\mathbf{D}_0^{el}$ is the initial (undamaged) elastic isotropic stiffness of the material, $\mathbf{D}^{el} = (1-d)\mathbf{D}_0^{el}$ is the degraded elastic stiffness of the material, and $\boldsymbol{\varepsilon}$ is the strain tensor. The effective stress is defined as:

$$\overline{\boldsymbol{\sigma}} \stackrel{\text{def}}{=} \mathbf{D}_0^{el}\left(\boldsymbol{\varepsilon} - \boldsymbol{\varepsilon}^{pl}\right), \tag{2.2}$$

where $\boldsymbol{\varepsilon}^{pl}$ is the plastic strain, then the scalar stiffness degradation variable is

$$d = d\left(\overline{\boldsymbol{\sigma}}, \widetilde{\varepsilon}^{pl}\right). \tag{2.3}$$

The scalar stiffness degradation variable is governed by a set of hardening variables $\widetilde{\varepsilon}^{pl}$. In the CDP model, the stiffness degradation is isotropic and defined by degradation variable d_c in a compression zone and variable d_t in a tension zone. Hence, the Cauchy stress tensor is related to the effective stress through $(1-d)$, which is scalar degradation relation. The effective stress can be formed as follows:

$$\boldsymbol{\sigma} = (1-d)\overline{\boldsymbol{\sigma}}, \tag{2.4}$$

where the factor $(1-d)$ shows the ratio of the effective load-carrying area (i.e., the total part minus the damaged part) to the total section area. When there is no damage, $d=0$, the effective stress $\overline{\boldsymbol{\sigma}}$ is equivalent to the Cauchy stress $\boldsymbol{\sigma}$. When damage arises, the Cauchy stress is not typical as much as the effective stress since it is resisting the external loads by the effective stress area [30]. The uniaxial compressive and tensile response of concrete (assumed to be influenced by damage plasticity) is given by:

$$\sigma_t = (1 - d_t) E_0 \left(\varepsilon_t - \widetilde{\varepsilon}_t^{pl} \right), \tag{2.5}$$

$$\sigma_c = (1 - d_c) E_0 \left(\varepsilon_c - \widetilde{\varepsilon}_c^{pl} \right). \tag{2.6}$$

By giving the nominal uniaxial stress, which determines the size of the yield (or failure) surface, the effective uniaxial cohesion stresses can be derived as:

$$\overline{\sigma}_t = \frac{\sigma_t}{(1 - d_t)} = E_0 \left(\varepsilon_t - \widetilde{\varepsilon}_t^{pl} \right), \tag{2.7}$$

$$\overline{\sigma}_c = \frac{\sigma_c}{(1 - d_c)} = E_0 \left(\varepsilon_c - \widetilde{\varepsilon}_c^{pl} \right). \tag{2.8}$$

The equivalent plastic strains may increase by the function of uniaxial degradation variables, ranging from 0 (undamaged) to 1 (fully damaged) [3]. As mentioned before, d_t and d_c are two independent uniaxial damage variables. They are also functions of the plastic strains, temperature, and field variables [30, 31]:

$$d_t = d_t \left(\widetilde{\varepsilon}_t^{pl}, \theta, f_i \right) \quad (0 \leq d_t \leq 1), \tag{2.9}$$

$$d_c = d_c \left(\widetilde{\varepsilon}_c^{pl}, \theta, f_i \right) \quad (0 \leq d_c \leq 1). \tag{2.10}$$

2.1. Abaqus documentation CDP material parameters, class B30

The Abaqus Verification Manual [1] provides CDP material parameters that are widely used. Table 1 lists those parameters and Fig. 1 shows the compressive and tensile behaviour.

Table 1. Abaqus material parameters for the CDP model [1].

Young's modulus [MPa]	Poisson's ratio	Mass density [kg/m^3]	Dilation angle	Eccentricity	f_{bo}/f_{co}	γ	Viscosity parameter
26480	0.167	2.4E–09	15	0.1	1.16	0.666	0
Compressive behaviour				Tensile behaviour			
Yield stress [MPa]	Inelastic strain	Damage parameter		Yield stress [MPa]	Cracking strain	Damage parameter	
24.019	0	0		1.78	0	0	
29.208	0.0004	0.1299		1.457	0.0001	0.3	
31.709	0.0008	0.2429		1.113	0.0003	0.55	
32.358	0.0012	0.3412		0.96	0.0004	0.7	
31.768	0.0016	0.4267		0.8	0.0005	0.8	
30.379	0.002	0.5012		0.536	0.0008	0.9	
28.507	0.0024	0.566		0.359	0.001	0.93	
21.907	0.0036	0.714		0.161	0.002	0.95	
14.897	0.005	0.8243		0.073	0.003	0.97	
2.953	0.01	0.9691		0.04	0.005	0.99	

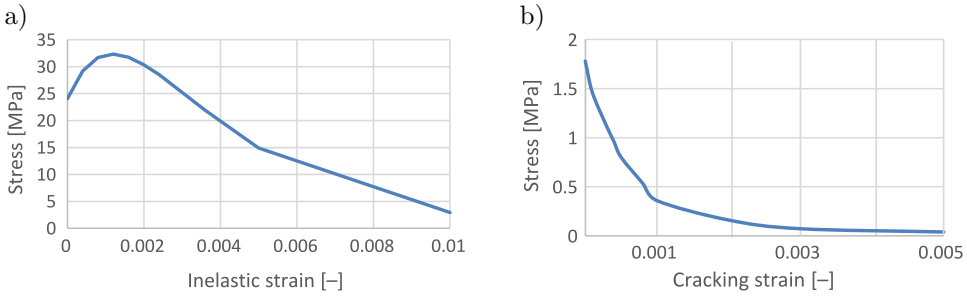

FIG. 1. The compressive and tensile behaviour of the Abaqus Documentation CDP material parameters, class B30: a) compressive behaviour, b) tensile behaviour.

2.2. HAFEZOLGHORANI *et al.* [3] *CDP material parameters, class B30 and B50*

HAFEZOLGHORANI *et al.* [3] developed simplified concrete damage plasticity (SCDP) model and listed CDP parameters for different classes of concrete. In this paper, the focus is on classes B30 and B50. Therefore, Table 2 presents the CDP material parameters for classes B30 and B50 presented in Figs. 2 and 3, respectively.

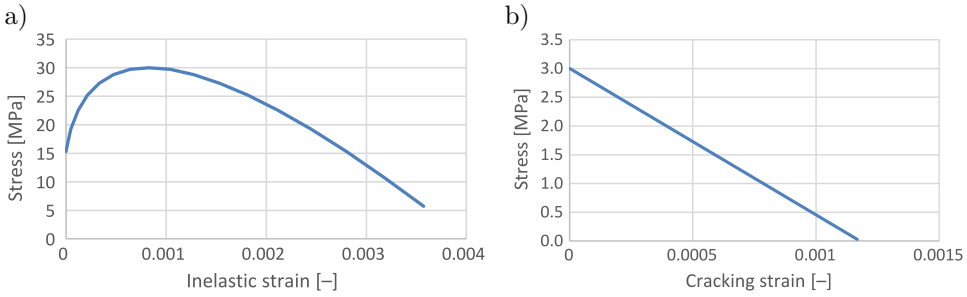

FIG. 2. The compressive and tensile behaviour of HAFEZOLGHORANI *et al.* [3] CDP material parameters, class B30: a) compressive behaviour, b) tensile behaviour.

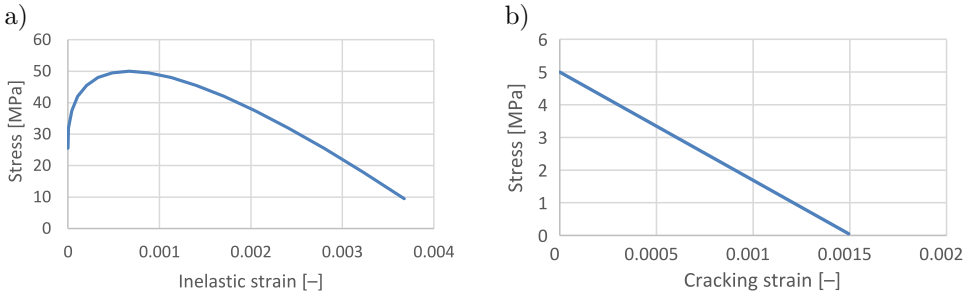

FIG. 3. The compressive and tensile behaviour of HAFEZOLGHORANI *et al.* [3] CDP material parameters, class B50: a) compressive behaviour, b) tensile behaviour.

Table 2. HAFEZOLGHORANI *et al.* [3] material parameters for the CDP model, class B30.

Class B30				Class B50			
Young's modulus [MPa]	Poisson's ratio	Dilation angle		Young's modulus [MPa]	Poisson's ratio	Dilation angle	
26600	0.2	31		33400	0.2	31	
Eccentricity	f_{bo}/f_{co}	K	Viscosity parameter	Eccentricity	f_{bo}/f_{co}	K	Viscosity parameter
0.1	1.16	0.67	0	0.1	1.16	0.67	0
Tensile behaviour				Tensile behaviour			
Yield stress [MPa]	Cracking strain	Damage parameter	Cracking strain	Yield stress [MPa]	Cracking strain	Damage parameter	Cracking strain
3	0	0	0	5	0.000000	0	0
0.03	0.00117	0.99	0.001167	0.05	0.001494	0.99	0.001494
Compressive behaviour				Compressive behaviour			
Yield stress [MPa]	Inelastic strain	Damage parameter		Yield stress [MPa]	Inelastic strain	Damage parameter	
15.3	0.000000	0		25.5	0.000000	0	
19.2	0.000048	0		32	0.000006	0	
22.5	0.000120	0		37.5	0.000041	0	
25.2	0.000215	0		42	0.000107	0	
27.3	0.000333	0		45.5	0.000202	0	
28.8	0.000475	0		48	0.000328	0	
29.7	0.000640	0		49.5	0.000483	0	
30	0.000828	0		50	0.000668	0	
29.7	0.001040	0.01		49.5	0.000883	0.01	
28.8	0.001275	0.04		48	0.001128	0.04	
27.3	0.001533	0.09		45.5	0.001402	0.09	
25.2	0.001815	0.16		42	0.001707	0.16	
22.5	0.002120	0.25		37.5	0.002041	0.25	
19.2	0.002448	0.36		32	0.002406	0.36	
15.3	0.002800	0.49		25.5	0.002800	0.49	
10.8	0.003175	0.64		18	0.003224	0.64	
5.7	0.003574	0.81		9.5	0.003678	0.81	

2.3. Jankowiak and Łodygowski [2] CDP material parameters, class B50

JANKOWIAK and ŁODYGOWSKI [2] CDP material parameters are also widely used by researchers. The proposed CDP parameters were based on numerical and experimental tests and can be used to model plain and RC structures, in

addition to pre-stressed concrete members. Table 3 shows material parameters for the CDP model proposed by Jankowiak and Łodygowski [2], while Fig. 4 presents the corresponding compressive and tensile behaviour.

Table 3. Jankowiak and Łodygowski [2] material parameters for the CDP model, class B50.

Young's modulus [MPa]	Poisson's ratio	Mass density [kg/m^3]	Dilation angle	Eccentricity ϵ	f_{bo}/f_{co}	K	Viscosity parameter
19700	0.19	2.3E–09	38	1	1.12	0.666	0.007985
Compressive behaviour				Tensile behaviour			
Yield stress [MPa]	Inelastic strain	Damage parameter		Yield stress [MPa]	Cracking strain	Damage parameter	
15.00	0.000000	0.0000		1.9989	0.000000	0.0000	
20.20	0.000075	0.0000		2.8420	0.000033	0.0000	
30.00	0.000099	0.0000		1.8698	0.000160	0.4064	
40.30	0.000154	0.0000		0.8627	0.000280	0.6964	
50.01	0.000762	0.0000		0.2263	0.000685	0.9204	
40.24	0.002558	0.1954		0.0566	0.001087	0.9801	
20.24	0.005675	0.5964					
5.26	0.011733	0.8949					

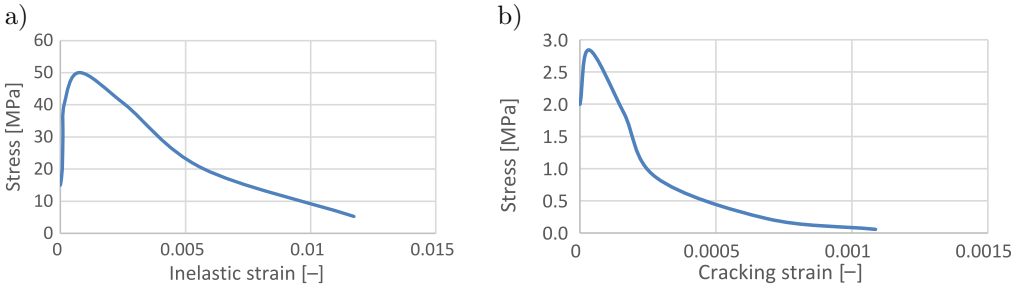

Fig. 4. The compressive and tensile behaviour of Jankowiak and Łodygowski [2] CDP material parameters, class B50: a) compressive behaviour, b) tensile behaviour.

A summary of the CDP material models used in this paper is shown in Table 4. On the other hand, the steel material of the supports and loading

Table 4. A summary of the CDP material models used in this paper.

CDP models	Author/source	Class	Abbreviated as
1	Abaqus documentation [1]	B30	CDP-1-B30
2	Hafezolghorani *et al.* [3]		CDP-2-B30
3	Hafezolghorani *et al* [3]	B50	CDP-3-B50
4	Jankowiak and Łodygowski [2]		CDP-4-B50

elements was assumed to have a density of 7850 kg/m^3, Young's modulus (E) of 200 000 MPa and Poisson's ratio (v) of 0.3. All steel material data were taken from Lovén and Svavarsdóttir [32].

3. Testing scheme/numerical model

3.1. Compressive strength test for concrete cube under (static) loading

The concrete cube was modelled as a 3-dimensional deformable body with a dimension of 150 mm according to the European standards presented in [33]. Additionally, a steel 3-dimensional deformable solid ($150 \times 150 \times 10$ mm) was used at the bottom of the concrete specimen as a support and on the top to apply the load through. The loading and supportive plates were modelled with C3D8I elements and were assigned rigid body constraints. Figure 5 shows the compressive strength testing scheme for the concrete cube. Moreover, Fig. 6 shows the numerical model and the dimensions. The assembly was made according to Chaudhari and Chakrabarti [17]. Similarly, parts that are not in our interest (top loading plate and lower supporting plate) were assumed as rigid bodies to reduce the computational time of the numerical model. Furthermore, the loading plate (Fig. 5) has a fixed BC in the initial step at its reference point. Then, movement in the y-direction was released when loaded. In addition, the supporting plate (Fig. 6) was completely fixed through its reference point, which means all translations and rotations were not allowed. The cube has an element type of 8-node linear brick element (C3D8I) with incompatible modes. The mesh size of 5 mm was chosen for the concrete specimen, which

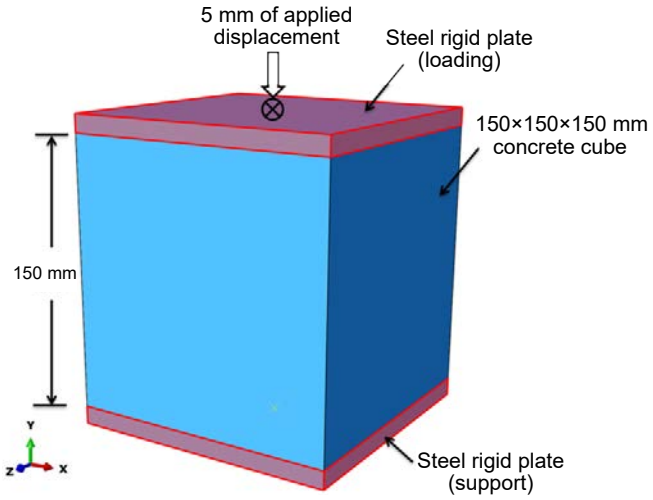

Fig. 5. The compressive strength testing scheme for the concrete cube.

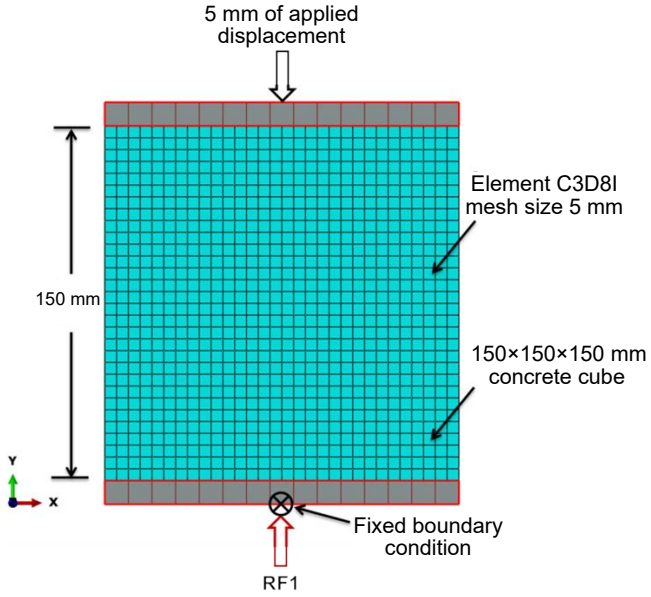

FIG. 6. The dimensions [mm] and numerical model of the compressive strength test for the concrete cube.

showed to be the more accurate/less expensive option. Additionally, the loading and supportive plates had a mesh size of 10 mm (which was not very important as the parts were assigned rigid body constraints). The "frictionless" tangential behaviour and "hard" normal behaviour were used to simulate the interaction between the concrete cube and supportive steel plates. As stated in the literature, "reducing friction is recommended to lower the strength variation" which "leads to more accurate and more economical concrete testing" [34].

3.2. Three-point flexural test for a plain concrete beam

The concrete beam was numerically modelled as a 3-dimensional deformable body using the Simulia Abaqus FE software. The beam has the standard sample dimensions ($750 \times 150 \times 150$ mm) according to the European standard [33]. Figure 7 shows the three-point flexural testing scheme for the considered plain concrete beam. Additionally, a 3-dimensional steel cylinder (with 50 mm diameter and 150 mm length) was used as two supports at the bottom and one at the top middle of the beam to apply the load through. As the behaviour/deformation of the cylinders was outside the scope of the research, they were assigned rigid body constraints that assumed complete rigidity of the cylinders. Figure 8 shows the dimensions [mm] and the numerical model. The parts were assembled with respect to standard specifications and the literature (such as the location of the

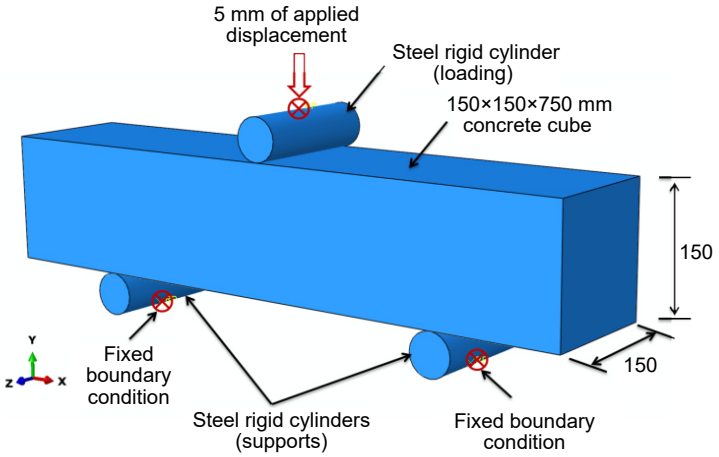

FIG. 7. The three-point flexural testing scheme for the plain concrete beam.

supports). Three boundary conditions were used in the present case. The supporting steel cylinders were fixed through their reference points, which means all translational and rotational degrees of freedom were restrained. On the other hand, the loading cylinder was fixed in all directions in the initial step, and then the movement in the y-direction was released to allow the corresponding vertical movement. The beam itself was restrained in the z-direction to prevent such a slip over the supports. The three boundary conditions mentioned above were used to replicate the experimental lab setup. An 8-node linear brick element (C3D8I) with incompatible modes was used for the concrete beam. The mesh size of 5 mm was the more accurate/less expensive model after checking different mesh sizes. Therefore, 5 mm was chosen for this concrete beam (Fig. 8). Addi-

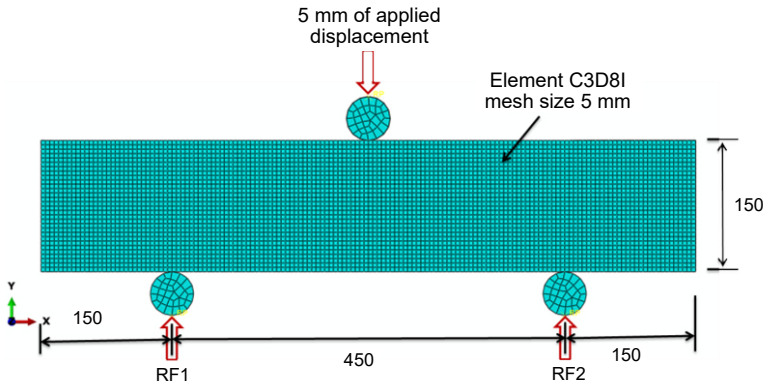

FIG. 8. The dimensions [mm] and the numerical model of the three-point flexural test for the plain concrete beam.

tionally, the loading and supportive cylinders had a mesh size of 10 mm (which was not very important as the parts were assigned rigid body constraints). The "frictionless" tangential behaviour and "hard" normal behaviour were used to simulate the interaction between the concrete cube and supportive steel cylinders.

3.3. Computational solver and comparative study

For the compressive strength and the three-point flexural tests, the computational analyses could not converge using a Static/Abaqus-standard solver. This is related to the fact that the computational model contains plasticity, damage and sophisticated contact between the steel cylinders/plates and concrete samples. Hence, an Abaqus/Explicit solver was chosen. The use of an explicit dynamic solver for a quasi-static analysis is well-presented in the literature and approved by the software documentation. According to the Abaqus documentation "*The explicit dynamics procedure is typically used to solve two classes of problems: transient dynamic response calculations and quasi-static simulations involving complex nonlinear effects (most commonly problems involving complex contact conditions*)" [30]. The time for the explicit step was set as 0.01 s to reduce the computational time required. For quasi-static simulations incorporating rate-independent material behaviour, the natural time scale is generally not important [1]. The explicit general contact was defined. To reduce the effects of undesirable inertia forces, at time $t = 0$, the steel plates/cylinders were located in contact with the concrete samples.

To compare the material parameters of the different CDP models (described in Sec. 2), a gradual displacement of 0–5 mm (with a 0.01 mm step interval) was applied to the concrete specimens through the upper reference points for both three-point flexural test and compressive strength test. By applying gradual displacement, observing the elasticity, plasticity and damage zones can be assured for those different classes of concrete and testing schemes. The results will compare the deformations, compression and tension damage patterns, reaction forces, compressive strength, tensile stress and modulus of rapture. For the compressive strength and the three-point flexural tests, the comparisons will be between the B30 class CDP models (CDP-1-B30 and CDP-2-B30), and between the B50 class CDP models (CDP-3-B50 and CDP-4-B50).

4. Results

4.1. Results of compressive strength test for concrete cube

The results of the compressive strength test of the concrete cube revealed interesting similarities and differences between the four considered CDP ma-

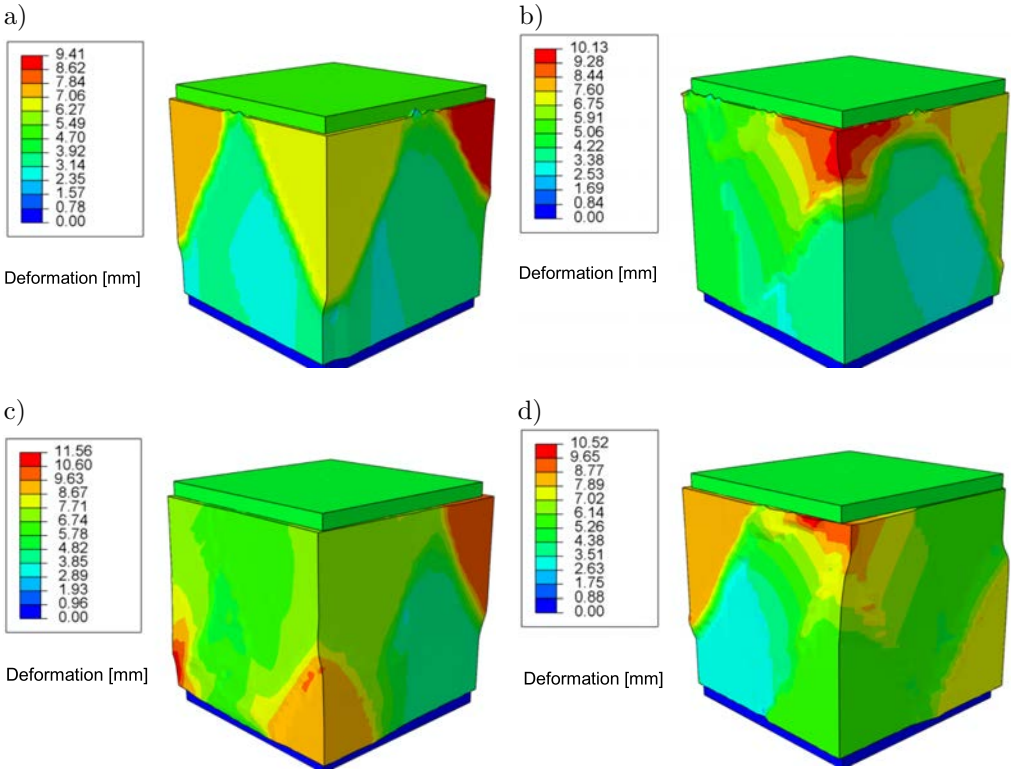

FIG. 9. The comparison between the four considered CDP models in terms of recorded deformation (in mm), resulting from the compressive strength test of a standard concrete cube at the applied displacement of 5 mm: a) CDP-1-B30, b) CDP-2-B30, c) CDP-3-B50, d) CDP-4-B50.

terial parameters. Figure 9 shows the comparison between the four considered CDP models in terms of maximum deformation resulting from the applied displacement of 5 mm. The deformation patterns of CDP-1-B30 (Fig. 9a) showed symmetry, with more deformations located in the top corners. However, the values are not symmetric, with a maximum deformation of 9.41 mm. Compared to CDP-2-B30 (Fig. 9b), the deformation pattern is random with an approximately similar peak deformation value of 10.13 mm ($\sim$0.7 mm of difference). By looking at the other two CDP models with the B50 class of concrete, the same conclusion can be drawn: although deformation patterns may differ, the peak deformation values are almost similar (with only $\sim$1 mm of difference), as shown in Figs. 9c and 9d.

The compression damage criteria and crack patterns were also compared at the applied displacement of 5 mm (Fig. 10). Diagonal crack patterns can be seen in CDP-1-B30 and CDP-4-B50, with approximately similar damage criteria of ($\sim$2.3). On the other hand, wider and more scattered cracks can be

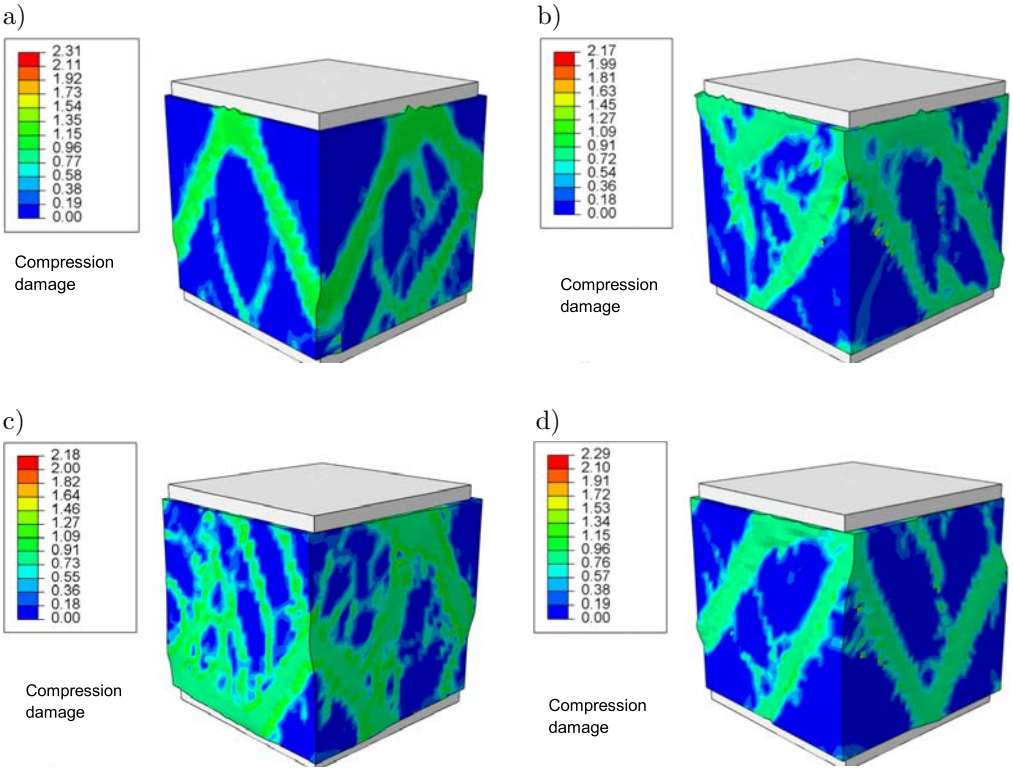

FIG. 10. The comparison between the four considered CDP models in terms of the compression damage criteria and crack patterns, resulting from the compressive strength test of a standard concrete cube at the applied displacement of 5 mm: a) CDP-1-B30, b) CDP-2-B30, c) CDP-3-B50, d) CDP-4-B50.

observed in CDP-2-B30 and CDP-3-B50 (the models proposed by HAFEZOLGHORANI *et al.* [3]) with similar damage criteria of (∼2.17).

It is also important to compare the four considered CDP models in terms of the load-deformation and corresponding stress-strain curves for the compressive strength of a concrete cube. Figure 11 shows the applied displacement versus corresponding nodal reaction force (RF) curves that compare the B30 material models (CDP-1-B30 and CDP-2-B30). The applied displacement represents the forced movement of the top steel plate compressing the concrete cube. The corresponding nodal reaction force, at the centre of the bottom steel supporting plate, is equivalent to the required applied load to cause such compression. Therefore, dividing the nodal RF by the concrete cube compressed area of 150×150 mm (22 500 mm^2) gives the compressive strength (in MPa). Moreover, dividing the applied displacement by the total height of the concrete cube (150 mm) gives the strain, based on which the corresponding stress-strain curves

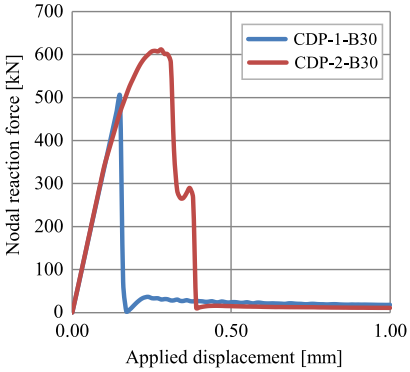

FIG. 11. Applied displacement versus corresponding nodal RF for the compressive strength of a concrete cube modeled with CDP-1-B30 and CDP-2-B30 material parameters.

are presented in Fig. 12. Results show that the compressive strength of CDP-1-B30 is 22.4 MPa compared to 27.2 MPa for the CDP-2-B30. In other words, none of the two models reached the 30 MPa specified compressive strength, with better performance for the CDP-2-B30 that showed a 9.3% discrepancy from the 30 MPa target. The non-linear behaviour of CDP-2-B30 is close to the one found by CHAUDHARI and CHAKRABARTI [17], who modelled the same cube for CDP-2-B30 material parameters. However, they used larger mesh sizes of 15, 18.75, and 25 mm, and showed that the smaller the mesh size, the less compressive strength is achieved. This can be linked to the fact that smaller FE elements can reach damage criteria faster than bigger elements, leading to quicker strength degradation.

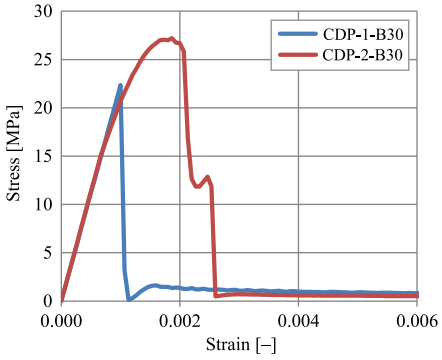

FIG. 12. The compressive strength stress-strain relationship for the concrete cube modelled with CDP-1-B30 and CDP-2-B30 material parameters.

On the other hand, the load-deformation curves (Fig. 13) and the corresponding stress-strain curves (Fig. 14) compare the B50 material models (CDP-3-B50 and CDP-4-B50). The CDP-3-B50 showed a maximum compressive strength of

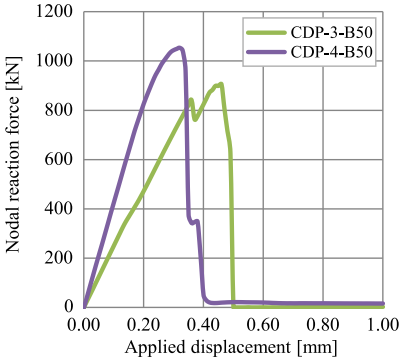

FIG. 13. Applied displacement versus corresponding nodal RF for the compressive strength of a concrete cube modeled with CDP-3-B50 and CDP-4-B50 material parameters.

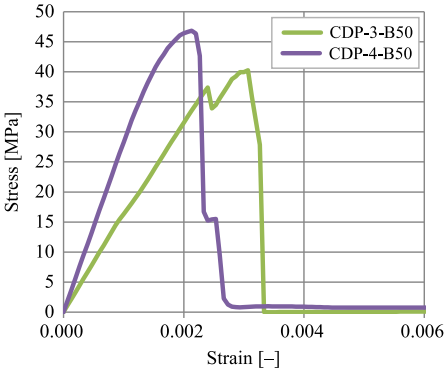

FIG. 14. The compressive strength stress-strain relationship for the concrete cube modelled with CDP-3-B50 and CDP-4-B50 material parameters.

40.3 MPa compared to 46.9 MPa for the CDP-4-B50, making the latter outperform other models with only a 6.2% discrepancy from the specified compressive strength target. It is worth mentioning that elastic, plastic and strength degradation stages were all within 0–0.5 mm/0–0.003 of applied displacement/strain, respectively.

Moreover, the compressive strength stress-strain relationships (Figs. 12 and 14) show particularly abrupt post-peak softening behaviour, almost like a brittle material. However, in reality, concrete is a quasi-brittle material with a more smooth, exponentially decaying stress-strain curve.

4.2. Results of three-point flexural test for a plain concrete beam

The results of this three-point flexural test for plain concrete beam consider the deformation, damage, maximum tensile stress, reaction forces and flexural

strength (Modulus of Rapture). Figure 15 shows the comparison between the four considered CDP models in terms of recorded deformation at the applied displacement of 5 mm. In contrast to the concrete cube compression test results, the deformation patterns (in the three-point flexural tests) of the CDP models are similar. Moreover, the B30 models (CDP-1-B30 and CDP-2-B30) showed 1.7 mm of peak deformation difference (Figs. 15a and 15b), compared to only 0.5 mm of peak deformation difference between CDP-3-B50 and CDP-4-B50 (Figs. 15c and 15d). The results reveal the consistency between the four CDP models.

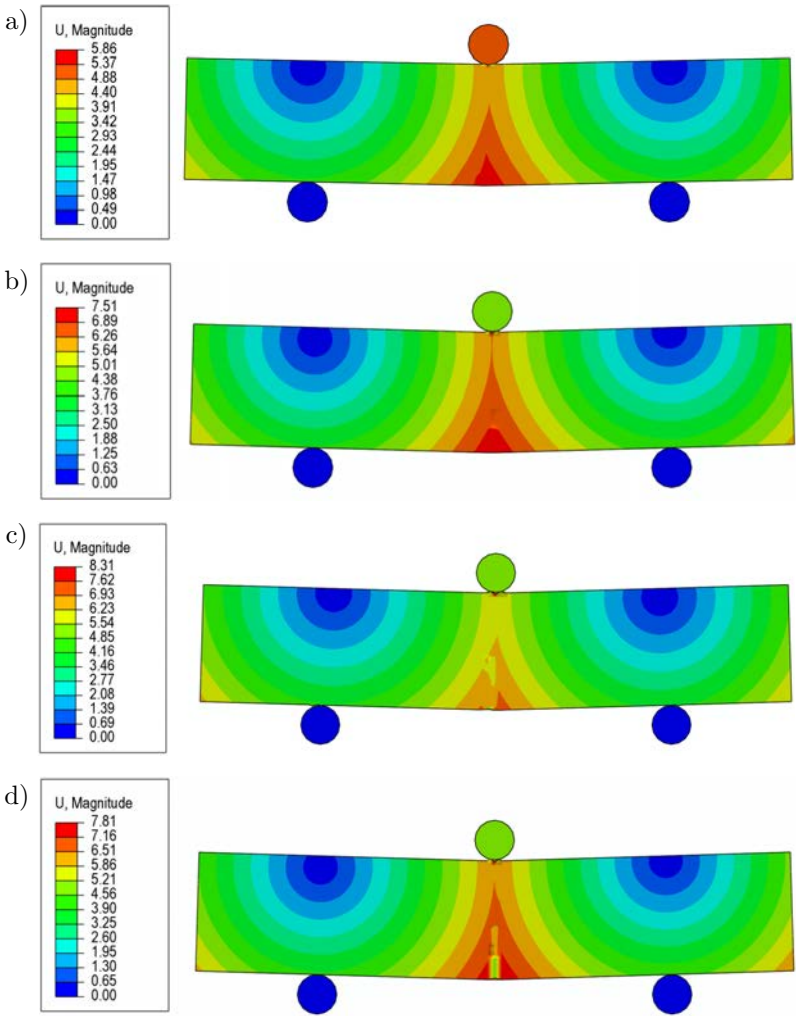

FIG. 15. The comparison between the four considered CDP models in terms of recorded deformation resulting from the three-point flexural test of a plain concrete beam at the applied displacement of 5 mm: a) CDP-1-B30, b) CDP-2-B30, c) CDP-3-B50, d) CDP-4-B50.

As the concrete beam is non-reinforced, the expected dominant damage pattern is tension damage with no shear cracks. This was shown by the tension damage outcomes presented in Fig. 16, where a linear crack propagates gradually from the bottom mid-span to the upper loading point.

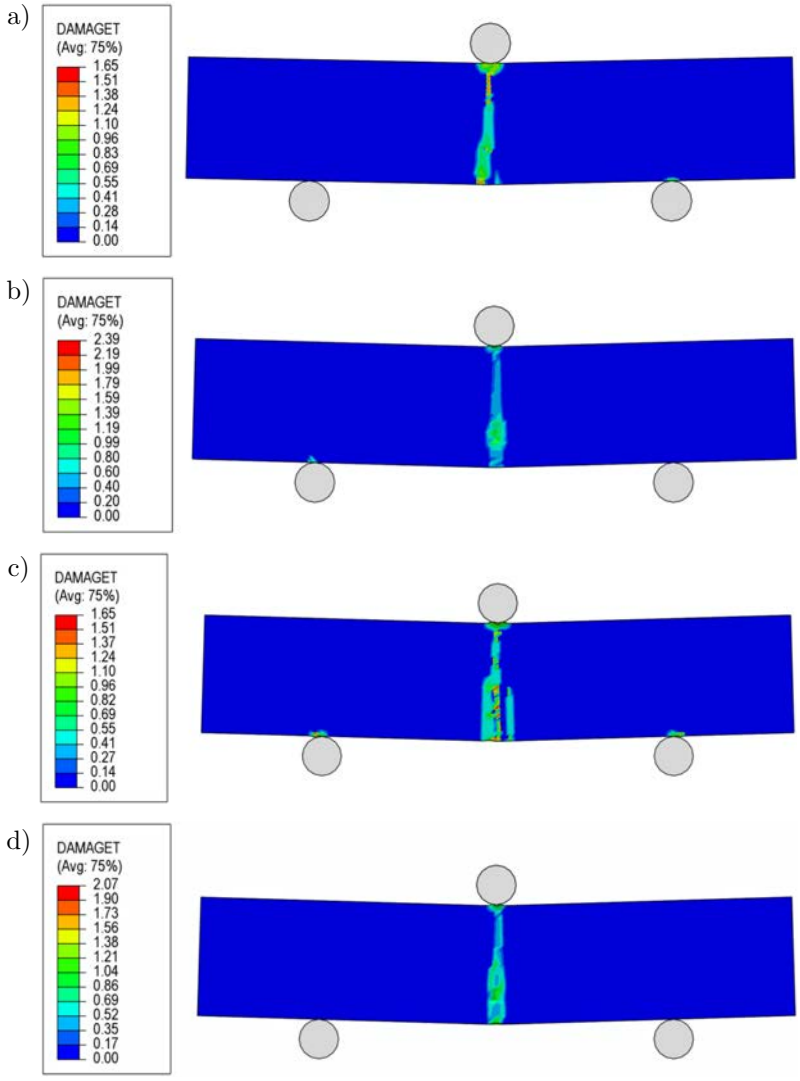

Fig. 16. The comparison between the four considered CDP models in terms of tension damage criteria and crack patterns resulting from the three-point flexural test of a plain concrete beam at the applied displacement of 5 mm: a) CDP-1-B30, b) CDP-2-B30, c) CDP-3-B50, d) CDP-4-B50.

Moreover, Fig. 17 shows the comparison between the four considered CDP models in terms of the maximum tensile stress (MPa) that the beam could

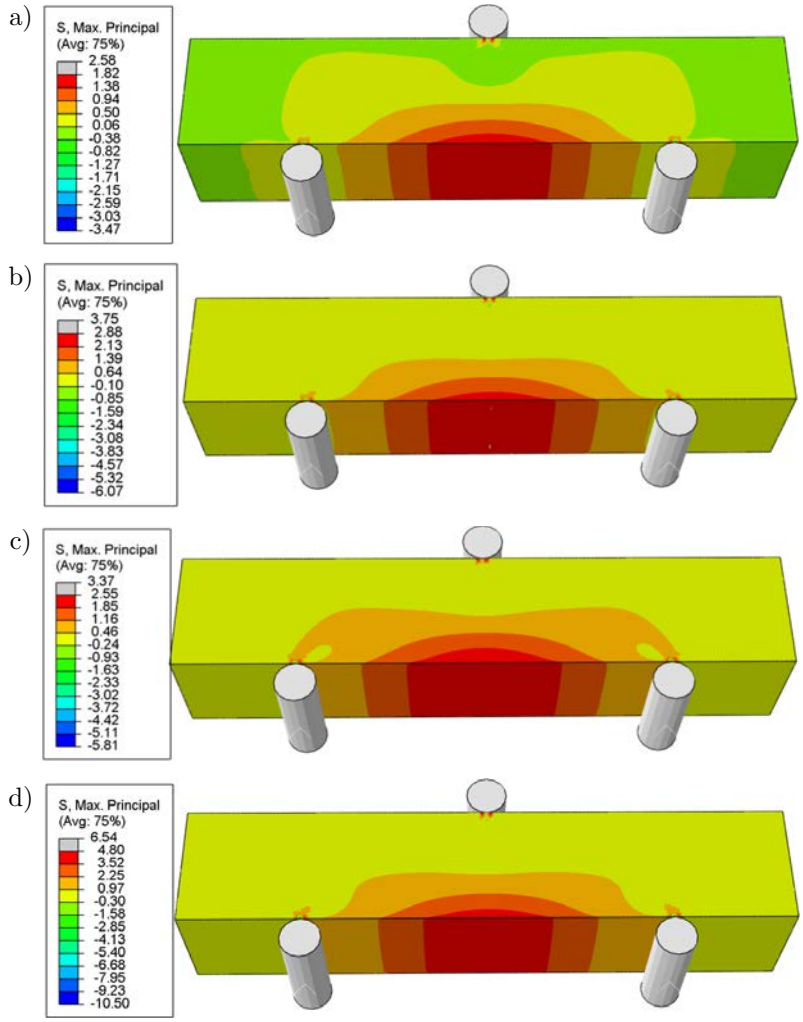

FIG. 17. The comparison between the four considered CDP models in terms of the maximum tensile stress resulting from the three-point flexural test of a plain concrete beam: a) CDP-1-B30, b) CDP-2-B30, c) CDP-3-B50, d) CDP-4-B50.

handle just before crack occurrence. According to Table 1, the maximum tensile stress of CDP-1-B30 is 1.78 MPa, while the tensile strength at the bottom fibres of the beam mid-span is 1.82 MPa (Fig. 17a). According to Table 2, the maximum tensile stress of CDP-2-B30 is 3 MPa, while the tensile strength at the bottom fibres of the beam mid-span is 2.88 MPa (Fig. 17b). The results show a good correlation between the assumed and obtained tensile strength for the B30 models.

On the other hand, according to Table 2, the maximum tensile stress of CDP-3-B50 is 5 MPa, while prior to the damage, the tensile strength at the bottom

fibres of the beam mid-span was only 2.55 MPa (Fig. 17c). Lastly, according to Table 3, the maximum tensile stress of CDP-3-B50 is 2.84 MPa, while the tensile strength at the bottom fibres of the beam mid-span is as high as 4.8 MPa (Fig. 17d). The results show inconsistency between the assumed and obtained tensile strength for the B50 models.

The applied displacement versus the sum of the corresponding nodal RFs (RF1+RF2) is presented in Fig. 18 (for the B30 material parameters) and in Fig. 19 (for the B50 material parameters). The brittle failure occurs at the applied displacement of less than 0.1 mm. The sum of the corresponding nodal vertical reaction forces is equivalent to the applied nodal force that would cause such a response. Hence, the peak values in Figs. 18 and 19 are considered the "maximum flexural load" that the beam can sustain. Figure 20 shows the com-

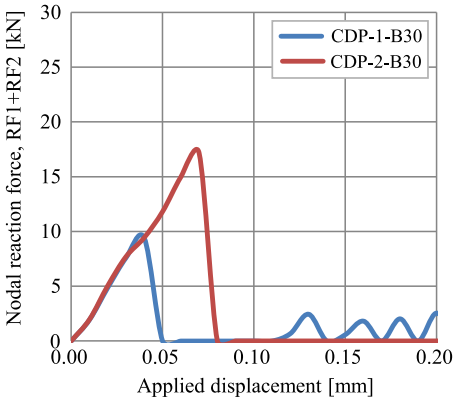

FIG. 18. Applied displacement versus corresponding nodal RFs (RF1+RF2) for the flexural strength of a concrete beam modelled with CDP-1-B30 and CDP-2-B30 material parameters.

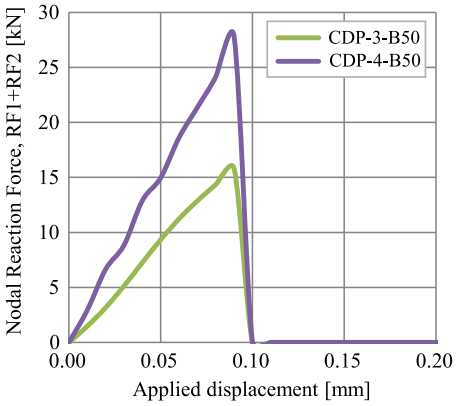

FIG. 19. Applied displacement versus corresponding nodal RFs (RF1+RF2) for the flexural strength of a concrete beam modelled with CDP-3-B50 and CDP-4-B50 material parameters.

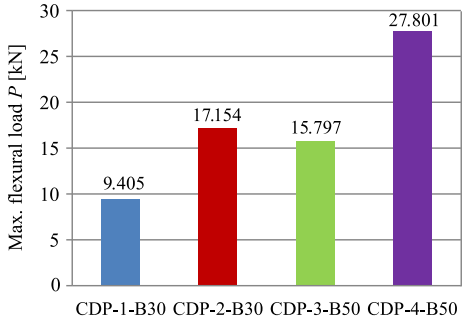

FIG. 20. The comparison between the four considered CDP models in terms of maximum flexural load (P) calculated from the summation of nodal RFs (RF1+RF2) of the plain concrete beam.

parison between the four considered CDP models in terms of maximum flexural load P, calculated from the summation of nodal RFs. According to the standard test method for flexural strength of concrete, the modulus of rapture R [MPa], can be calculated as:

$$R = 3\frac{PL}{2bd^2}, \tag{4.1}$$

where P is the maximum flexural load N, L is the clear span length (450 mm), b is the width of the specimen (150 mm), and d is the depth of the specimen (150 mm). Figure 21 shows the comparison between the four considered CDP models in terms of modulus of rapture R calculated using Eq. (4.1) and maximum flexural load (P) presented in Fig. 20. It can be noticed that R for CDP-1-B30 is quite different than that of CDP-2-B30, making CDP-1-B30 more conservative. The same noticeable difference can be seen for the B50 models, as CDP-4-B50 is almost double that of CDP-3-B50. In spite of the difference in classes of concrete material, CDP-2-B30 and CDP-3-B50 showed close values of maximum flexural load and modulus of rapture. This can be linked to

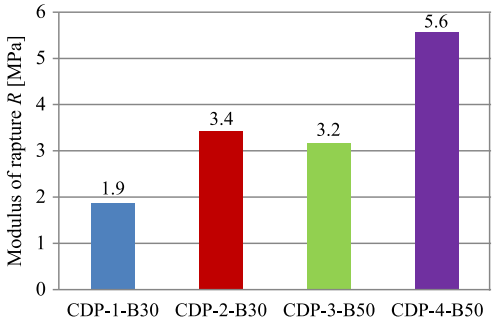

FIG. 21. The comparison between the four considered CDP models in terms of modulus of rapture R [MPa] calculated using Eq. (4.1) and maximum flexural load P presented in Fig. 20.

the fact that they are both proposed by the same authors [3] using the same formulations.

5. Conclusions

This research conducted a comparative assessment of four commonly-used concrete CDP parameters by assessing the response of plain concrete specimens under quasi-static loading conditions. Assumptions included, but were not limited to, the use of the Abaqus/Explicit solver for rate-independent material models to replicate the quasi-static loading conditions. The following can be concluded from the numerical FE tests:

1) Compressive strength test:
   - Deformations: The deformation patterns of the four compared CDP parameters are random with close values of peak deformations.
   - Compression damage: Diagonal crack patterns can be observed in CDP-1-B30 and CDP-4-B50, while wider and more scattered cracks can be observed in CDP-2-B30 and CDP-3-B50 (the models proposed by Hafezolghorani *et al.* [3]).
   - Compressive strength: The compressive strength of CDP-1-B30 was 22.4 MPa compared to 27.2 MPa for the CDP-2-B30 that showed less discrepancy from the 30 MPa target. The CDP-3-B50 showed a maximum compressive strength of 40.3 MPa compared to 46.9 MPa for the CDP-4-B50, making the latter outperform other models with only a 6.2% discrepancy from the specified compressive strength target.
2) Three-point flexural test:
   - Deformations: The deformation patterns for the four CDP material parameters were similar. Moreover, the B30 models showed 1.7 mm of peak deformation difference, compared to only 0.5 mm of peak deformation difference between CDP-3-B50 and CDP-4-B50. The results reveal the consistency between the four CDP models.
   - Tensile damage: As the concrete beam is non-reinforced, the dominant damage for all CDP material parameters was tension damage in the form of a vertical crack in the middle span of the beam.
   - Maximum tensile stress: The results show a good correlation between the assumed and obtained tensile strength values for the B30 models, although the B50 models revealed inconsistency.
   - Modulus of rapture: The maximum flexural load and the corresponding modulus of rapture for the four CDP models showed a noticeable difference, although the CDP-2-B30 and CDP-3-B50 showed close values in spite of the difference in classes of concrete material.

In short, the critical analyses presented here conclude that choosing CDP parameters is case-sensitive and should be selected carefully. The authors' future interest is to assess the response of the four CDP material parameters to impact loading conditions, which could be the main limitation of this paper.

Conflict of interest

The authors declare no conflict of interest.

Funding

Partial financial support was received from the Ministry of Science and Higher Education, Poland, grant number 0411/SBAD/0004.

References

1. Dassault Systèmes, *Abaqus 6.10 Verification Manual*, Simulia Corp., Providence, RI, USA, 2010.

2. Jankowiak T., Łodygowski T., Identification of parameters of concrete damage plasticity constitutive model, *Foundations of Civil and Environmental Engineering*, **6**(1): 53–69, 2005.

3. Hafezolghorani M., Hejazi F., Vaghei R., bin Jaafar M.S., Karimzade K., Simplified damage plasticity model for concrete, *Structural Engineering International*, **27**(1): 68–78, 2018, doi: 10.2749/101686616X1081.

4. Adekeye A.W., Awoyera P., Strength characteristics of concrete beams reinforced with steel bars of equivalent area but different diameters, *Research Journal of Applied Sciences, Engineering and Technology*, **11**(7): 765–769, 2015, doi: 10.19026/rjaset.11.2039.

5. Hillerborg A., Modéer M., Petersson P-E., Analysis of crack formation and crack growth in concrete by means of fracture mechanics and finite elements, *Cement and Concrete Research*, **6**(6): 773–781, 1976, doi: 10.1016/0008-8846(76)90007-7.

6. Sümer Y., Aktaş M., Defining parameters for concrete damage plasticity model, *Challenge Journal of Structural Mechanics*, **1**(3): 149–155, 2015, doi: 10.20528/cjsmec.2015.07.023.

7. Tao Y., Chen J-F., Concrete damage plasticity model for modeling FRP-to-concrete bond behavior, *Journal of Composites for Construction*, **19**(1): 04014026, 2014, doi: 10.1061/(ASCE)CC.1943-5614.0000482.

8. Alongi A., Angelotti A., Mazzarella L., A numerical model to simulate the dynamic performance of Breathing Walls, *Journal of Building Performance Simulation*, **14**(2): 155–180, 2021, doi: 10.1080/19401493.2020.1868578.

9. Hillerborg A., The theoretical basis of a method to determine the fracture energy G_F of concrete, *Materials and Structures*, **18**(4): 291–296, 1985, doi: 10.1007/BF02472919.

10. Al-Rifaie H., Sumelka W., Numerical analysis of a reinforced concrete supporting structure for blast resistant gates, [in:] *23rd International Conference on Computer Methods in Mechanics PCM-CMM*, Kraków, Poland 2019.

11. Al-Rifaie H., Sumelka W., Numerical analysis of reaction forces in blast resistant gates, *Structural Engineering and Mechanics*, **63**(3): 347–359, 2017, doi: 10.12989/sem.2017.63.3.347.

12. Al-Rifaie H., Studziński R., Gajewski T., Malendowski M., Peksa P., Sumelka W., Sielicki P.W., Full scale field testing of trapezoidal core sandwich panels subjected to adjacent and contact detonations, [in:] Giżejowski M.A., Kozłowski A., Chybiński M., Rzeszut K., Studziński R., Szumigała M. [Eds.], *Modern Trends in Research on Steel, Aluminium and Composite Structures: Proceedings of the XIV International Conference on Metal Structures (ICMS2021)*, Poznań, Poland, 16–18 June 2021, London: Routledge 2021, pp. 393–399, doi: 10.1201/9781003132134.

13. Cüneyt Aydin A., Tortum A., Yavuz M., Prediction of concrete elastic modulus using adaptive neuro-fuzzy inference system, *Civil Engineering and Environmental Systems*, **23**(4): 295–309, 2007, doi: 10.1080/10286600600772348.

14. Al-Rifaie H., Sumelka W., Auxetic damping systems for blast vulnerable structures, [in:] Voyiadjis G.Z. [Ed.], *Handbook of Damage Mechanics*, pp. 1–23, Springer, New York, NY, 2020, doi: 10.1007/978-1-4614-8968-9_71-1.

15. Szczecina M., Winnicki A., Calibration of the CDP model parameters in Abaqus, *The 2015 World Congress on Advances in Structural Engineering and Mechanics (ASEM15)*, Incheon, Korea, 2015.

16. Fedoroff A., Calonius K., Kuutti J., Behavior of the Abaqus CDP model in simple stress states, *Rakenteiden Mekaniikka*, **52**(2): 87–113, 2019, doi: 10.23998/rm.75937.

17. Chaudhari S.V., Chakrabarti M., Modeling of concrete for nonlinear analysis using finite element code ABAQUS, *International Journal of Computer Applications*, **44**(7): 14–18, 2012, doi: 10.5120/6274-8437.

18. Wahalathantri B., Thambiratnam D., Chan T., Fawzia S., A material model for flexural crack simulation in reinforced concrete elements using ABAQUS, [in:] Cowled C.J.L. [Ed.], *Proceedings of the First International Conference on Engineering, Designing and Developing the Built Environment for Sustainable Wellbeing*, pp. 260–264, Queensland University of Technology, Australia, 2011.

19. Ren W., Sneed L.H., Yang Y., He R., Numerical simulation of prestressed precast concrete bridge deck panels using damage plasticity model, *International Journal of Concrete Structures and Materials*, **9**(1): 45–54, 2015, doi: 10.1007/s40069-014-0091-2.

20. Farahmandpour C., Dartois S., Quiertant M., Berthaud Y., Dumontet H., A concrete damage–plasticity model for FRP confined columns, *Materials and Structures*, **50**(2): 1–17, 2017, doi: 10.1617/s11527-017-1016-8.

21. Majed M.M., Tavakkolizadeh M., Allawi A.A., Finite element analysis of rectangular RC beams strengthened with FRP laminates under pure torsion, *Structural Concrete*, **22**(4): 1946–1961, 2021, doi: 10.1002/suco.202000291.

22. Othman H., Marzouk H., Applicability of damage plasticity constitutive model for ultra-high performance fibre-reinforced concrete under impact loads, *International Journal of Impact Engineering*, **114**: 20–31, 2018, doi: 10.1016/j.ijimpeng.2017.12.013.

23. Banyhussan Q.S., Yildirim G., Anil Ö., Erdem R.T., Ashour A., Şahmaran M., Impact resistance of deflection-hardening fiber reinforced concretes with different mixture parameters, *Structural Concrete*, **20**(3): 1036–1050, 2019, doi: 10.1002/suco.201800233.

24. Kakavand M.R.A., Taciroglu E., An enhanced damage plasticity model for predicting the cyclic behavior of plain concrete under multiaxial loading conditions, *Frontiers of Structural and Civil Engineering*, **14**(6): 1531–1544, 2020, doi: 10.1007/s11709-020-0675-7.

25. Plos M., Gylltoft K., Evaluation of shear capacity of a prestressed concrete box girder bridge using non-linear FEM, *Structural Engineering International*, **16**(3): 213–221, 2006, doi: 10.2749/101686606778026457.

26. Lubliner J., Oliver J., Oller S., Oñate E., A plastic-damage model for concrete, *International Journal of Solids and Structures*, **25**(3): 299–326, 1989, doi: 10.1016/0020-7683(89)90050-4.

27. Lee J., Fenves G.L., Plastic-damage model for cyclic loading of concrete structures, *Journal of Engineering Mechanics*, **124**(8): 892–900, 1998, doi: 10.1061/(ASCE)0733-9399(1998)124:8(892).

28. Malm R., *Shear cracks in concrete structures subjected to in-plane stresses*, Licentiate dissertation, KTH Royal Institute of Technology, Sweden 2006, http://urn.kb.se/resolve?urn=urn:nbn:se:kth:diva-4215.

29. Fedoroff A., Calonius K., Using the Abaqus CDP model in impact simulations, *Rakenteiden Mekaniikka*, **53**(3): 180–207, 2020, doi: 10.23998/rm.79723.

30. Dassault Systèmes, *Abaqus Analysis User Manual*, Vol. 4, Simulia Corp. Providence, RI, USA, 2007.

31. Al-Rifaie H., *Application of passive damping systems in blast resistant gates*, PhD Thesis, Poznan University of Technology, Poznan, 2019.

32. Lovén J., Svavarsdóttir E.S., *Concrete beams subjected to drop weight impact-comparison of experimental data and numerical modelling*, Master's Thesis in the Master's Programme Structural Engineering and Building Technology, Chalmers University of Technology, Göteborg, Sweden, 2016.

33. CEN-EN 12390-1, *Testing hardened concrete – Part 1: Shape, dimensions and other requirements for specimens and moulds*, European Committee for Standardization, 12 pages, 2021.

34. Talaat A., Emad A., Tarek A., Masbouba M., Essam A., Kohail M., Factors affecting the results of concrete compression testing: A review, *Ain Shams Engineering Journal*, **12**(1): 205–221, 2021, doi: 10.1016/j.asej.2020.07.015.

Received November 3, 2021; accepted version May 6, 2022.